

Ultralow-threshold two-photon pumped amplified spontaneous emission and lasing from seeded CdSe/CdS nanorod heterostructures

Xing, Guichuan; Liao, Yile; Wu, Xiangyang; Chakraborty, Sabyasachi; Liu, Xinfeng; Yeow, Edwin Kok Lee; Sum, Tze Chien; Chan, Yinthai

2012

Xing, G., Liao, Y., Wu, X., Chakraborty, S., Liu, X., Yeow, E. K. L., et al. (2012). Ultralow-threshold two-photon pumped amplified spontaneous emission and lasing from seeded CdSe/CdS nanorod heterostructures. *ACS Nano*, 6 (12), 10835–10844.

<https://hdl.handle.net/10356/95297>

<https://doi.org/10.1021/nn304200a>

© 2012 American Chemical Society. This is the author created version of a work that has been peer reviewed and accepted for publication by ACS Nano, American Chemical Society. It incorporates referee's comments but changes resulting from the publishing process, such as copyediting, structural formatting, may not be reflected in this document. The published version is available at: [DOI: <http://dx.doi.org/10.1021/nn304200a>].

Downloaded on 15 Jul 2024 18:36:28 SGT

Ultralow Threshold Two-Photon Pumped Amplified Spontaneous Emission and Lasing from Seeded CdSe/CdS Nanorod Heterostructures

Guichuan Xing, Yile Liao, Xiangyang Wu, Sabyasachi Chakraborty, Xinfeng Liu, Edwin K. L. Yeow, Yinthal Chan, and Tze Chien Sum

ACS Nano, **Just Accepted Manuscript** • Publication Date (Web): 17 Nov 2012

Downloaded from <http://pubs.acs.org> on November 19, 2012

Just Accepted

“Just Accepted” manuscripts have been peer-reviewed and accepted for publication. They are posted online prior to technical editing, formatting for publication and author proofing. The American Chemical Society provides “Just Accepted” as a free service to the research community to expedite the dissemination of scientific material as soon as possible after acceptance. “Just Accepted” manuscripts appear in full in PDF format accompanied by an HTML abstract. “Just Accepted” manuscripts have been fully peer reviewed, but should not be considered the official version of record. They are accessible to all readers and citable by the Digital Object Identifier (DOI®). “Just Accepted” is an optional service offered to authors. Therefore, the “Just Accepted” Web site may not include all articles that will be published in the journal. After a manuscript is technically edited and formatted, it will be removed from the “Just Accepted” Web site and published as an ASAP article. Note that technical editing may introduce minor changes to the manuscript text and/or graphics which could affect content, and all legal disclaimers and ethical guidelines that apply to the journal pertain. ACS cannot be held responsible for errors or consequences arising from the use of information contained in these “Just Accepted” manuscripts.



1
2
3
4
5
6
7
8
9
10
11
12
13
14
15
16
17
18
19
20
21
22
23
24
25
26
27
28
29
30
31
32
33
34
35
36
37
38
39
40
41
42
43
44
45
46
47
48
49
50
51
52
53
54
55
56
57
58
59
60

Ultralow Threshold Two-Photon Pumped Amplified Spontaneous Emission and Lasing from Seeded CdSe/CdS Nanorod Heterostructures

*Guichuan Xing,^{†,§} Yile Liao,^{‡,§} Xiangyang Wu,[□] Sabyasachi Chakraborty,[‡] Xinfeng Liu,[†]
Edwin K. L. Yeow,[□] Yinthai Chan,^{‡, ⊥, *} and Tze Chien Sum^{†, *}*

[†]Division of Physics and Applied Physics, School of Physical and Mathematical Sciences,
Nanyang Technological University, 21 Nanyang Link, Singapore 637371

[‡]Department of Chemistry, National University of Singapore, 3 Science Drive 3, Singapore
117543

[⊥]Institute of Materials Research & Engineering, A*STAR, 3 Research Link, Singapore 117602

[□]Division of Chemistry and Biological Chemistry, School of Physical and Mathematical
Sciences, Nanyang Technological University, 21 Nanyang Link, 637371

*Address correspondence to : tzechien@ntu.edu.sg; chmchany@nus.edu.sg

1
2
3 **ABSTRACT** Ultralow threshold two-photon pumped amplified spontaneous emission (2ASE)
4 and lasing in seeded CdSe/CdS nanodot/nanorod heterostructures is demonstrated for the first
5 time. Such heterostructures allow the independent tunability of the two-photon absorption (2PA)
6 cross-section (σ_2) through varying the CdS rod size, and that of the emission wavelength through
7 varying the CdSe dot size. With an enhanced σ_2 , 2ASE in these heterostructures is achieved with
8 an ultralow threshold fluence of $\sim 1.5 \text{ mJ/cm}^2$ – which is as much as one order less than that
9 required for spherical semiconductor NCs. Importantly, by exploiting this unique property of the
10 seeded nanorods exhibiting strong quantum confinement even at relatively large rod sizes, a near
11 reciprocal relation between the 2ASE threshold and the 2PA action cross-section ($\sigma_2\eta$) (where η
12 is the quantum yield) was found and validated over a wide volume range for II-VI semiconductor
13 nanostructures. Ultrafast optical spectroscopy verified that while the Auger processes in these
14 heterostructures are indeed suppressed, ASE in these samples could also be strongly affected by a
15 fast hole trapping process to the NR surface states. Lastly, to exemplify the potential of these
16 seeded CdSe/CdS nanodot/nanorod heterostructures as a viable gain media for achieving two-
17 photon lasing, a highly photostable microsphere laser with an ultralow pump threshold is
18 showcased.

19
20
21
22
23
24
25
26
27
28
29
30
31
32
33
34
35
36
37
38
39
40
41
42
43
44
45
46 **KEYWORDS:** CdSe/CdS nanorod, upconversion, Whispering Gallery mode lasing, two-photon
47 absorption, ultrafast,
48
49
50
51
52
53
54
55
56
57
58
59
60

1
2
3 Colloidal semiconductor nanocrystals (NCs) are desirable as optical gain media due to their
4 excellent photostability, continuous tunability over a wide spectral range and easy chemical
5 processability.¹⁻¹⁷ These advantageous physicochemical properties make NCs highly suited for
6 optical applications such as multi-wavelength on-chip microcavity lasers and as miniaturized light
7 sources in lab-on-a-chip diagnostics.¹⁻¹⁶ To date, optically pumped amplified spontaneous
8 emission (ASE) and lasing in colloidal semiconductor NCs have largely been demonstrated using
9 one-photon excitation (1PE) with ultraviolet/visible light sources.¹⁻¹² However, it is foreseeable
10 that in many of the applications for which NC lasers are relevant, the use of UV-Vis excitation
11 wavelengths risk the high possibility of photo-damage to the sample and substrate, or unwanted
12 excitation of fluorescent contaminants present in the application setup. A promising route to the
13 derivation of ASE and lasing in NCs while circumventing the above issues is optical pumping
14 *via* two-photon excitation (2PE) at infrared (IR) wavelengths.¹²⁻¹⁶

15
16
17
18
19
20
21
22
23
24
25
26
27
28
29
30
31
32
33
34
35
36
37
38
39
40
41
42
43
44
45
46
47
48
49
50
51
52
53
54
55
56
57
58
59
60
2PE is achieved through the simultaneous absorption of two photons that induces an electronic
transition from the ground state to an excited state *via* virtual states. In contrast to 1PE, 2PE
possesses several unique features such as higher spatial resolution and longer penetration depth
when operating in the semi-transparent infrared window of biological media, and has thus been
exploited for bio-imaging.^{12-16,18-21} Additionally, for the generation and wavelength tuning of
coherent light, the absence of a phase matching requirement in the 2PE process makes it highly
attractive over other nonlinear frequency conversion techniques (*e.g.*, optical harmonic
generation) as this permits its application to a much wider range of resonator designs and gain
media (other than birefringent crystalline materials).¹²⁻¹⁶ Given the advent of robust, low-cost,
versatile and compact IR laser sources (*e.g.*, fiber lasers), 2PE has become a viable technique for
the generation of coherent light *via* the attainment of optical gain in colloidal semiconductor
NCs.

1
2
3 One major impediment to the development of practical two-photon pumped colloidal
4 semiconductor NC lasers is the small two-photon absorption (2PA) cross-section (typically
5 $\sigma_2 \approx 10^{-46}$ cm⁴/photon) for most spherical core-(thin) shell II-VI semiconductor NCs that
6 necessitate the use of high laser excitation fluences to derive optical gain. Thus, prior efforts to
7 achieve two-photon induced stimulated emission in NCs typically resulted in very high
8 thresholds of over 10 mJ/cm².¹²⁻¹⁶ For 2PE, the average number of electron-hole (e-h) pairs
9 created by each laser pulse is given as $\langle N_2 \rangle = f^2 \sigma_2 / \tau_p$, where f is the fluence and τ_p is the pulse
10 duration. For a fixed τ_p , it is desirable to increase σ_2 and reduce f for the same $\langle N_2 \rangle$ in order to
11 reduce the likelihood of photo-damage to the gain media. While simply increasing the volume of
12 strongly confined NCs to increase σ_2 appears to be a straight-forward solution, an increase in size
13 for these strongly quantum confined NCs inevitably red shifts their band-edge fluorescence,
14 thereby imposing severe limitations on their spectral tunability. For the fabrication of devices
15 with wavelength specific requirements such as lasers, this presents a formidable challenge.

16
17
18
19
20
21
22
23
24
25
26
27
28
29
30
31
32
33
34
35
36 Herein we demonstrate that these issues may be simultaneously addressed using seeded
37 CdSe/CdS nanorod (NR) heterostructures, which comprise of a spherical CdSe core that is
38 encapsulated by a rod-like CdS shell as the optical gain media. While the CdS shell functions as
39 an antenna in light harvesting, emission from the rod originates primarily from the quantum
40 confined CdSe core.^{8,22-25} This unique optical configuration thus allows for σ_2 and the emission
41 wavelength to be varied independently by adjusting the physical dimensions of the rod-like shell
42 and spherical core respectively. We then show that *via* the use of highly monodisperse CdSe
43 seeded CdS NRs, room temperature ASE *via* 2PE at 800 nm can be obtained with thresholds as
44 low as 1.5 mJ/cm². The NRs were subsequently incorporated into a silica matrix and coupled to a
45 microspherical cavity where single mode lasing at a threshold of 0.99 mJ/cm² was derived. At
46
47
48
49
50
51
52
53
54
55
56
57
58
59
60

1
2
3 such low pump intensities, lasing from the NRs *via* 2PE was stable over the course of 6×10^6
4
5 laser shots under ambient conditions, thus making these NC laser devices plausible for use in
6
7 practical applications. Ultrafast optical spectroscopy (UOS) also revealed that while the
8
9 nonradiative Auger recombination processes ($\tau_{\text{Auger}} \sim 200 - 300$ ps) are indeed suppressed in
10
11 these NR heterostructures, the ASE could still be strongly affected by the ultrafast hole trapping
12
13 to the NR surface.
14
15
16
17

18 19 **Results and Discussion**

20
21 In this work, seeded CdSe/CdS NR heterostructures of three different rod lengths (*i.e.* 15 nm,
22
23 34 nm and 39 nm) with the same CdSe core (~ 2.4 nm) were investigated. The size of the CdSe
24
25 core (< 2.8 nm) indicates that these rods are expected to exhibit a quasi-type II core-shell energy
26
27 profile.²⁴ The photoluminescence (PL) quantum yield (QY) of these NRs in toluene were
28
29 measured to be 0.75, 0.61 and 0.56, respectively. Their structure and basic optical properties are
30
31 shown in Fig. 1. These NR samples in toluene were spin casted onto glass slides to form close-
32
33 packed thin films of NRs, with thicknesses of ~ 500 nm. The surface roughness of these films was
34
35 characterized using tapping-mode atomic force microscopy which yielded typical root-mean-
36
37 square roughness values of ~ 6 nm measured over a $2 \mu\text{m} \times 1 \mu\text{m}$ scan area.
38
39
40
41

42
43 Optical gain in Type-I colloidal semiconductor NCs is generally achieved with the generation
44
45 of multiexcitons due to the spin degeneracy in its first excited state. For example, due to a two-
46
47 fold degeneracy in the $1S_e-1S_h$ transition of CdSe NCs, biexcitons are required in order to derive
48
49 optical gain.^{1,26} The 2PA cross-section σ_2 thus becomes an important metric in determining the
50
51 photon flux required to generate biexcitons *via* 2PE and subsequently achieve stimulated
52
53 emission. In the case of ASE from NC-based waveguides, it is fairly obvious that increasing
54
55 σ_2 without exacerbating other key parameters such as NC volume fraction, Auger recombination
56
57
58
59
60

1
2
3 rates and waveguide Q-factors would result in lower threshold fluences. The relationship
4 between the PLQY and that of the ASE threshold, however, can be rather complex. On the one
5 hand, the PLQY may not be as important a factor compared to the extremely fast Auger
6 recombination rates if its non-radiative contribution is comparatively slower. On the other hand,
7 the PLQY is a reflection of the degree of passivation of the NC surface, which has been shown
8 by several reports to be strongly related to Auger recombination processes in the NC.^{27,28}
9
10 Furthermore, given that the carriers are generated primarily in the CdS shell and then undergo
11 charge transfer to the CdSe core in these NR heterostructures, carrier trapping processes to the
12 NR surface states can also be a highly efficient non-radiative pathway that competes effectively
13 with both ASE and Auger recombination processes. Finally, the single exciton PLQY is likely to
14 play a role in the provision of seed photons for the photon cascade that occurs in ASE. Hence, to
15 take into account the contributions from these factors, we use the two-photon action cross-section
16 (*i.e.* $\sigma_2 \times \eta$) of the NC sample as a basis for analyzing the relationship between the threshold
17 fluence and σ_2 .
18
19
20
21
22
23
24
25
26
27
28
29
30
31
32
33
34
35
36
37

38 **Determination of 2PA Cross-sections**

39 As the two-photon pumped ASE of the NR films is strongly dependent on the nonlinear
40 absorption properties of the CdSe seeded CdS NRs, we first determined the 2PA cross-sections
41 (σ_2) of these NR heterostructures using the open aperture Z-scan technique with 150 fs laser
42 pulses (1 KHz) at a wavelength of 800 nm.²⁰ Table 1 lists the σ_2 values measured for samples
43 with different rod lengths, which can ostensibly be described as exhibiting a superlinear
44 dependence. Elucidating the physical origins of this superlinear dependence is non-trivial though
45 it is likely due to the local field effects on the nanostructure size and the density of states.¹⁸⁻²⁰ For
46 39 nm long NRs, a σ_2 value of 2.3×10^5 GM (where 1 GM = 10^{-50} cm⁴/s/photon) was measured,
47
48
49
50
51
52
53
54
55
56
57
58
59
60

1
2
3 which is two to four orders of magnitude larger than that previously reported for spherical
4 semiconductor QDs and about four orders of magnitude larger than that of typical organic
5 dyes.¹⁸⁻²⁰ Importantly, σ_2 can be varied independently of the CdSe core whose size primarily
6 determines the emission wavelength. The advantages of size dependent emission afforded by the
7 quantum confined CdSe core are therefore preserved in these heterostructures.
8
9
10
11
12
13
14

15 16 17 **Two-Photon Pumped Amplified Spontaneous Emission**

18 Figures 3(a) – (c) show the normalized room temperature emission spectra below and above
19 the two-photon pumped ASE (2ASE) threshold for 15 nm, 34 nm and 39 nm long CdSe seeded
20 CdS NRs with a CdSe core size of ~ 2.4 nm respectively. Following 2PA that is dominated by
21 the CdS shell, electron-hole pairs are formed and undergo ultrafast charge localization to the
22 CdSe core within ~ 1 ps, where radiative recombination occurs.^{8,25} Below the threshold fluence,
23 the two-photon pumped spontaneous emission (SE) of the heterostructures dominate the light
24 output with a bandwidth of ~ 40 nm (*i.e.* full width at half maximum (FWHM)). These spectra
25 are indistinguishable from the 1PE PL spectra shown in Fig. 1. Above this threshold, the
26 emission bandwidth reduced to less than 12 nm for all the samples, as a result of gain-induced
27 narrowing. Notably, the 2ASE peaks of all the samples are blue-shifted with respect to the
28 exciton peak with energy separations of 10 meV, 29 meV and 47 meV for the 15 nm, 34 nm and
29 39 nm NR heterostructures, respectively. The origins of this blue shift may be attributed to the
30 quasi-type II band alignment between the CdSe core and CdS shell (valid for CdSe core sizes $<$
31 2.8 nm²²⁻²⁵), which results in a negative biexciton binding energy (repulsive exciton-exciton
32 interaction) that causes its radiative recombination to occur at a higher energy than that of the
33 single exciton.^{1,4,7,26} This repulsive interaction increases with the length of the NR, and stems
34 from a decreased overlap of the electron-hole wavefunctions due to an increased electron
35
36
37
38
39
40
41
42
43
44
45
46
47
48
49
50
51
52
53
54
55
56
57
58
59
60

1
2
3 wavefunction delocalization into the rod-like shell. The resulting reduced attractive electron-hole
4 interaction is subsequently commensurate with a stronger repulsive interaction between charges
5 in the core and shell.^{1,4,7,26} It should be noted that it is unlikely that single exciton 2ASE from
6 these heterostructures was obtained since the biexciton repulsion energy is much smaller than the
7 ensemble linewidth of the single-exciton emission (*i.e.*, ~130 meV).⁷ Within quasi-type II band
8 alignment of the CdSe/CdS heterostructure, the 2ASE peak should be tunable between ~550 nm
9 and ~600 nm by tailoring the CdSe core and CdS shell size.^{11,22,24}

10
11
12
13
14
15
16
17
18
19
20 Figure 4(a) shows the dependence of the integrated PL intensity on the pump fluence. At
21 relatively low pump intensities (*i.e.*, <1.2 mJ/cm²), the PL emission shows a near quadratic pump
22 intensity dependence for all the samples, which validates the 2PA process at 800 nm.^{20,29} At
23 higher pump intensities, an abrupt change of the slope occurs, indicating a threshold behavior
24 that is characteristic of 2ASE. The 2ASE threshold pump intensities for the 15 nm, 34 nm and 39
25 nm CdSe/CdS heterostructures were found to be 3.4, 1.8 and 1.5 (mJ/cm²), respectively, for
26 samples with comparable film thicknesses (~ 500 nm) and loading fraction (~ 30%).¹⁵ It is
27 evident that the 2ASE threshold pump fluence decreases with increasing rod length, which may
28 be attributed to the increased σ_2 . The 2ASE threshold pump intensities as a function of the
29 heterostructures' 2PA action cross-section ($\sigma_2\eta$) are presented in Fig. 4(b). The plot summarizes
30 the experimental results from this study as well as those collated from the literature.^{14,15} From the
31 fit, the 2ASE threshold pump intensities exhibit a power-law dependence of -0.5 ± 0.1 to $\sigma_2\eta$. It
32 shows that the 2ASE threshold is nearly inversely proportional to $\sigma_2\eta$ (*i.e.*, a near reciprocal
33 relation), which is consistent with the notion that the enhanced 2PA cross-section at 800 nm due
34 to the CdS rod-like shell would effectively lower the pump intensities needed to achieve ASE.
35
36
37
38
39
40
41
42
43
44
45
46
47
48
49
50
51
52
53
54
55
56
57
58
59
60
Within our range of samples measured, the 39 nm long CdSe seeded CdS NRs have the largest

1
2
3 2PA action cross-section and yielded, to the best of our knowledge, the lowest 2ASE threshold to
4 date (*i.e.* $\sim 1.5 \text{ mJ/cm}^2$) for a colloidal NC system. Comparatively, this value is as much as one
5 order less than that obtained for spherical quantum dots.^{14,15} We emphasize that this comparison
6 is based on the achievement of ASE in a waveguide geometry, where unlike in the case of lasing
7 in optical cavities, the thresholds obtained are less strongly dependent on cavity Q-factors and
8 modal volumes. Based on the 2PA cross-sections measured with the Z-scan technique, the
9 number of electron-hole pairs generated per NC at threshold pump fluence are estimated to be
10 approximately 1.3, 1.1 and 1.0 for 15 nm, 34 nm and 39 nm long CdSe seeded CdS NRs,
11 respectively. This result is consistent with previous observations that the NR optical gain derives
12 primarily from the generation of biexcitons.¹⁻¹⁶

27 28 **Transient Optical Spectroscopy**

29 Time resolved two-photon excited PL experiments at room temperature were also performed
30 on the NR films in order to investigate the biexciton modal gain dynamics in these
31 heterostructures. Typical time-resolved three-dimensional (3D) plots of the 2PA induced SE and
32 ASE spectra for the 15 nm CdSe/CdS heterostructures are shown in Fig. 5(a) and 5(b),
33 respectively, while the emission decay curves for all the samples and their corresponding decay
34 fits are shown in Fig. 5 (c) (*i.e.* extracted at the peak of the excitonic emission and photoexcited
35 with a pump fluence of $\sim 0.1 \text{ mJ/cm}^2$). It is readily seen that the time dynamics of 2PA induced
36 SE are similar to that of 1PE and the intensity decays with time *via* a single exponential function,
37 with fitted decay lifetimes for the 15 nm, 34 nm and 39 nm rods at 10 ns, 12 ns and 14 ns,
38 respectively. These fitted lifetimes show that the exciton PL lifetimes increase with increasing
39 rod length, in accordance with the decrease in the CdSe electron-hole wave-function overlap due
40 to more extensive delocalization of the electron wavefunction in the longer rods. However,
41
42
43
44
45
46
47
48
49
50
51
52
53
54
55
56
57
58
59
60

1
2
3 compared to an ensemble of relatively isolated NRs in a dilute solution (*i.e.* in a solvent –
4 $\tau_{solution} \sim 20$ ns), the lifetimes obtained for these close packed films are slightly shorter – likely
5
6 due to dipole-mediated energy transfer processes between neighboring rods.³⁰ The energy
7
8 transfer time (τ_{ET}) is estimated to be around tens of ns with $1/\tau_{film} = 1/\tau_{solution} + 1/\tau_{ET}$.
9
10 Therefore, the dipole-dipole interaction between neighboring rods in our film is not expected to
11
12 have any significant effect on the 2ASE threshold. (2ASE occurs on a much faster time scale as
13
14 shown below).
15
16
17
18
19

20 At pump fluences above threshold for the 15 nm rod sample, a short-lived, spectrally narrow
21
22 emission band emerges at energies higher than that of the 2PA induced SE peak, as shown in
23
24 Figure 5(b). Figure 5(d) shows its luminescence decay profile at the peak wavelength of the ASE
25
26 transition for pump fluences below (*i.e.*, ~ 3 mJ/cm²) and above threshold (*i.e.*, ~ 3.5 mJ/cm²). It
27
28 should be noted that at the high pump fluence of ~ 3 mJ/cm², this is already in the regime of
29
30 multi-exciton generation, even though the fluence is just below the threshold needed for ASE.
31
32 Therefore, the PL decay dynamics exhibit a short lifetime component of ~ 200 ps, which is much
33
34 shorter than the typical ~ 10 ns excitonic recombination lifetimes for these NRs. This 200 ps
35
36 relaxation time closely matches the Auger-limited biexciton recombination lifetimes in these
37
38 CdSe/CdS heterostructures; which were probed using ultrafast transient absorption (TA)
39
40 spectroscopy and these results will be presented in the next paragraph. Beyond the threshold
41
42 fluence of ~ 3.5 mJ/cm², an even shorter fitted lifetime component of ~ 7 ps dominates the
43
44 radiative recombination dynamics, in addition to the ~ 200 ps Auger-limited biexciton
45
46 recombination lifetime. This even faster lifetime component is due to the ASE resulting from an
47
48 avalanche of biexcitonic recombination, where its lifetime measurements are limited by the
49
50 system temporal response of the streak camera.
51
52
53
54
55
56
57
58
59
60

1
2
3
4
5
6
7
8
9
10
11
12
13
14
15
16
17
18
19
20
21
22
23
24
25
26
27
28
29
30
31
32
33
34
35
36
37
38
39
40
41
42
43
44
45
46
47
48
49
50
51
52
53
54
55
56
57
58
59
60

Optical gain in semiconductor NCs is strongly dependent on the competition between radiative and non-radiative processes (*i.e.*, multiexciton Auger recombination, fast charge carrier trapping *e.t.c.*). Therefore, it is very important to elucidate and gain a clear understanding of the dynamic interplay between the various carrier relaxation channels through TA spectroscopy. Figure 6(a) shows representative differential transmittance (DT) spectra of these CdSe/CdS heterostructures (in toluene) at probe delay of 2 ps following 3.1 eV photoexcitation. The photobleaching (PB) peaks (*i.e.* $\Delta T/T > 0$) evident in the DT spectra arise from the state-filling of the hole-states in the CdSe core and the electron states in the CdS shell. These correspond to the lowest lying energy levels in the CdSe and CdS system and are labeled as X_0 and Y_0 , respectively.^{8,23,25} With increasing NR length, the amplitude ratio of X_0 to Y_0 decreases, consistent with an increased absorption from the larger rod-like shell. Pump-power dependent bleaching kinetics at X_0 was performed to elucidate the biexciton Auger recombination lifetimes in these NR heterostructures. Figure 6(b) shows the representative decay transients for the 15 nm NRs for different pump powers (expressed as an average number of electron-hole pairs). Using a procedure previously reported by Klimov *et. al.*,²⁶ the biexciton Auger recombination lifetimes were extracted and are shown in the inset of Figure 6(b). These were fitted to be 190, 260 and 300 ps for the 15 nm, 34 nm and 39 nm rods, respectively; which are much longer than the biexciton lifetime (*i.e.*, ~ 45 ps) for 2.3 nm CdSe spherical dots.²⁶ Hence, it may be inferred that the biexcitonic Auger recombination rates are indeed greatly suppressed in these NR heterostructures. The slower rates found in the longer rods are consistent with the decrease in the CdSe electron-hole wavefunction overlap caused by the more extensive delocalization of the electron wavefunction in the longer rods. However, compared to CdSe NRs of similar volume, the biexciton Auger rate is slightly faster in these heterostructures. We attribute this to the strong confinement of the holes in the CdSe core (in our heterostructures) and a more weakly confined electron which delocalizes into

1
2
3 the CdS shell. Hence, it is understandable that the Auger dynamics in this system of mixed
4
5 dimensionality are in-between the case of a zero dimensional quantum dot and that of a one-
6
7 dimensional quantum rod.²⁶ Further experimental investigations and theoretical modeling are
8
9 underway to gain a clearer understanding of the Auger processes that occur in these
10
11 heterostructures of mixed dimensionalities. In these CdSe/CdS NR heterostructures where the
12
13 Auger rates are suppressed, the optical gain build-up time compares favorably with the non-
14
15 radiative Auger processes.
16
17
18

19
20 In light of the fact that the suppressed Auger processes may not play a dominant role in the
21
22 ultrafast multiexciton dynamics of our 2PE derived ASE from CdSe/CdS NRs, we examined the
23
24 dynamics of other possible non-radiative processes, in particular ultrafast charge trapping to
25
26 surface states and their impact on the ASE process. As discussed previously, the relationship
27
28 between PLQY and the ASE threshold is complicated. If the PLQY is limited by the ultrafast
29
30 non-radiative surface trapping processes, it will play a bigger role than previously envisaged for
31
32 these mixed-dimensionality heterostructures and this provides a strong justification for our use of
33
34 $\sigma_2\eta$ as a basis for analyzing the relationship between threshold fluence and σ_2 . Furthermore, our
35
36 ASE threshold measurements show that the 2ASE threshold is nearly inversely proportional to
37
38 $\sigma_2\eta$ in the CdSe/CdS NR heterostructures, which indicates that the PLQY (dependent on the NR
39
40 length) is indeed limited by some ultrafast non-radiative processes (*i.e.*, other than Auger
41
42 recombination). The presence of the ultrafast non-radiative surface trapping processes can be
43
44 confirmed through TA spectroscopy.
45
46
47
48
49

50
51 Figure 7(a) shows the representative normalized bleaching kinetics at X_0 and Y_0 with fs time
52
53 resolution for the 39 nm NRs upon photoexcitation with a pump fluence of approximately 1
54
55 electron-hole (e-h) pair per rod. Following 1PA at 3.1 eV (or 2PA at 1.55 eV), e-h pairs are
56
57 primarily generated in the CdS shell. This results in an ultrafast build up of the PB transients (at
58
59
60

1
2
3 Y_0) that occur in a timescale comparable to the pulse width of the femtosecond laser (*i.e.*, ~150
4 fs). Following fast hole localization from the CdS shell to the CdSe core, the fast build up of the
5
6 PB transient at X_0 is simultaneously matched with an equally fast PB decay at Y_0 occurring
7
8 within 1 ps. The ensuing PL emission originates from the radiative recombination between the
9
10 strongly localized hole in the core and delocalized electron in the NR shell.^{8,22-25} Due to the
11
12 limitations in temporal resolution (*i.e.* ~ 150 fs) of our fs laser and that of the delay line of the fs-
13
14 TAS setup (*i.e.*, a maximum of ~ 6 ns, though ~ 3 ns is typically used), it may be difficult to
15
16 elucidate the evidence of the such surface/trap states from fs-TAS alone. A complimentary
17
18 approach to validating the presence of such non-radiative surface/trap states in the CdS shell
19
20 would be to examine the recovery of the system back to the equilibrium condition (on a much
21
22 longer timescale, *i.e.*, tens of ns to μ s) – with nanosecond (ns-)TA spectroscopy. Figure 7(b)
23
24 shows the ns-TA kinetics at Y_0 and X_0 , where the PB dynamics clearly show a prolonged
25
26 recovery of the PB signals back to the equilibrium for Y_0 (*i.e.*, CdS shell) while those of X_0 has
27
28 already decayed. The lifetime of the fast PB decay component for both Y_0 and X_0 coincides with
29
30 the PL lifetime of the heterostructures in toluene. Hence, we attribute this long PB lifetime in Y_0
31
32 to arise from the non-recovery of the electrons in the lowest CdS energy levels back to the
33
34 equilibrium. This can be attributed to the presence of some holes still being trapped at the CdS
35
36 surface states. Considering the high PLQY for these heterostructures (*i.e.*, > 50%), we can further
37
38 infer that the trapping to these surface hole states would have occurred on a timescale slightly
39
40 longer than the hole relaxing to the CdSe core (*i.e.* within a few ps), which is comparable to
41
42 surface hole trapping lifetimes reported in the literature for other NCs and NRs.³¹⁻³³ This
43
44 assignment is consistent with the rod length dependent PLQY measurements where the PLQY
45
46 decreases with increasing rod length. The longer of the NR, the higher the possibility of the holes
47
48 being trapped at the surface states as they migrate to the CdSe core. The long decay of Y_0
49
50
51
52
53
54
55
56
57
58
59
60

1
2
3 represents the slow recombination between the surface localized holes with delocalized electrons
4 in the NR. Due to the reduced wavefunction overlap between localized hole and the delocalized
5 electron in the longer NR, one would expect that the recombination lifetimes would increase as
6 the NR length increases. This is indeed validated by the results in the inset of Figure 7(b).
7
8 Nevertheless, despite that the fast surface hole trapping time is comparable with the timescales of
9 the biexcitonic recombination avalanche that triggers the ASE, low ASE thresholds can still be
10 achieved due to the large cross-sections and high PLQY (*i.e.*, action cross-sections) of these NR
11 heterostructures.
12
13
14
15
16
17
18
19
20
21

22 **Lasing from a Spherical Cavity**

23 We demonstrate the potential of these CdSe/CdS NRs as a gain medium for two-photon
24 pumped lasing using a spherical optical cavity. Such optical cavities can potentially possess
25 extremely high Q factors because of the strong confinement of photons within a given modal
26 volume.^{34,35} The CdSe/CdS NRs described above were chemically functionalized and
27 incorporated into sol-gel derived silica matrix to permit the adhesion of a thin layer of NRs-silica
28 onto the exterior of commercially available silica microspheres (with diameter of $5.0 \pm 0.3 \mu\text{m}$).
29 The motivation to put NRs-silica composites over silica sphere instead of NRs directly attached
30 to spheres is to increase the damage tolerance of samples to continuous pulsed excitation. Fig
31 8(a) shows an optical image of a typical NR-coated microsphere under optical excitation. Under
32 two-photon (800 nm) pumping, single-mode threshold lasing from the NR-coated microsphere
33 was achieved as shown in Fig 8(b). The laser line exhibits a FWHM ~ 0.75 nm with a Q factor of
34 ~ 800 (*i.e.* the Q factor is defined as $\lambda/\Delta\lambda$, where λ and $\Delta\lambda$ are the wavelength and the FWHM of
35 the laser emission). This value is consistent with previously reported values in similar cavities
36 under one-photon pumping,⁶ and may be attributed to the self-absorption of NRs, scattering from
37
38
39
40
41
42
43
44
45
46
47
48
49
50
51
52
53
54
55
56
57
58
59
60

1
2
3 structural defects within the film and surface roughness. Figures 8(c) and 8(d) show the threshold
4 behavior for two-photon pumped lasing in comparison to one-photon pumped lasing. The
5 threshold fluences are 910 ± 50 and $12 \pm 2 \mu\text{J}/\text{cm}^2$ for two-photon and one-photon pumped lasing
6 respectively. The ratio of their threshold fluence is ~ 100 , which is typical of those for two-photon
7 to one-photon pumped lasing.¹²⁻¹⁶ While slightly lower 2PA lasing thresholds for NCs in
8 spherical optical resonators have previously been reported,¹⁶ it should be recognized that such
9 thresholds are a strong function of the cavity Q-factor which is likely to differ significantly from
10 our setup. It should be noted that increasing the size of the NR shell not only increases σ_2 , but
11 also that of the one-photon absorption cross-section. Nonetheless, compared to spherical
12 semiconductor QDs under similar experimental conditions, both the one-photon and two-photon
13 pumped lasing thresholds are dramatically lowered in these NRs.¹²⁻¹⁶ Lastly, the photostability of
14 our prototype microsphere laser was evaluated by monitoring the lasing intensity as a function of
15 time under a continuous irradiation at a 1 KHz repetition rate under ambient conditions. Figures
16 8(e) and 8(f) show the variation in lasing intensity over 5×10^6 laser shots under one-photon and
17 two-photon pumping respectively. Following such a large number of laser pulse excitation
18 events, the near invariance of the output intensity for both cases bear testimony to the excellent
19 optical stability of the microsphere laser with the CdSe/CdS nanodot/nanorod heterostructures as
20 gain media.

46 47 **Conclusions**

48 In summary, ultralow threshold two-photon pumped ASE and lasing with CdSe/CdS
49 nanodot/nanorod heterostructures was demonstrated for the first time. Essentially, these NR
50 heterostructures afford us the means to independently tune the 2PA cross-section using the CdS
51 shell and the quantum confined emission wavelengths using the CdSe core. Using these NRs as
52
53
54
55
56
57
58
59
60

1
2
3 the gain media, the greatly enhanced σ_2 allows us to achieve 2ASE in thin film samples with an
4
5 ultralow threshold pump fluence of 1.5 mJ/cm² for the 39 nm NRs, which is as much as one order
6
7 less than that needed for 2ASE of spherical quantum dots. Importantly, by exploiting the unique
8
9 property of the seeded NRs to exhibit strong quantum confinement even at relatively large rod
10
11 sizes, a near inverse proportional dependence of the 2ASE threshold on the $\sigma_2\eta$ was found and
12
13 validated over a wide volume range for II-VI semiconductor nanostructures. New insight into the
14
15 charge dynamics of these NR heterostructures was also uncovered through UOS techniques. Our
16
17 investigations revealed that while the 2ASE ($\tau \leq 7$ ps) can effectively compete with the
18
19 suppressed Auger process ($\tau_{\text{Auger}} \sim 200$ ps) in these NR heterostructures, the 2ASE could be
20
21 strongly affected by the competition between hole localization to the CdSe core ($\tau \sim 1$ ps) and to
22
23 CdS surface states ($\tau > 1$ ps). Lastly, to demonstrate the potential of these NR heterostructures as
24
25 a viable gain media for achieving 2PE lasing, a high stability prototypical microsphere laser with
26
27 ultralow pump threshold was showcased.
28
29
30
31
32
33
34
35

36 Experimental Section

37 Seeded CdSe/CdS NRs heterostructures of different rod lengths were prepared according to a
38
39 previously published procedure²² with slight modifications. Briefly, spherical CdSe cores of ~ 2.4
40
41 nm in size were first synthesized *via* the hot injection method as described in reference²³,
42
43 followed by seeded growth of the CdS rod-like shell of different lengths at ~ 360 °C.
44
45

46 For femtosecond optical spectroscopy, the laser source was a Coherent LegendTM regenerative
47
48 amplifier (150 fs, 1 KHz, 800 nm) that was seeded by a Coherent MiraTM oscillator (100 fs, 80
49
50 MHz). 800 nm wavelength laser pulses were from the regenerative amplifier's output while 400
51
52 nm wavelength laser pulses were frequency doubled with a BBO crystal.
53
54
55
56
57
58
59
60

1
2
3 For Z-scan measurements, the incident laser pulses were focused onto the sample by a lens
4 with 30 cm focal length. The NR heterostructures in toluene solution were placed in 2 mm thick
5 quartz cell, which was traversed across the focal point along the beam propagation axis.
6
7

8
9
10 For femtosecond TA experiments, the samples were pumped at 3.1 eV and probed with white-
11 light continuum. The probe pulses (400-750 nm) were generated by focusing a small portion (~5
12 μJ) of the fundamental 800 nm laser pulses into a 1 mm-thick sapphire plate. The linear
13 polarization of the pump pulse was adjusted to be perpendicular to that of the probe pulse with a
14 polarizer and a half waveplate. The cross-polarization will help eliminate any contribution from
15 coherent artifacts at early times. Pump-induced changes of transmission ($\Delta T/T$) of the probe
16 beam were monitored using a monochromator/PMT configuration with lock-in detection. The
17 pump beam was chopped at 83 Hz and this was used as the reference frequency for the lock-in
18 amplifier.
19
20
21
22
23
24
25
26
27
28
29
30

31 For 2ASE experiments, the 800 nm laser pulses were focused by a cylindrical lens (with focal
32 length $f = 20$ cm) to a stripe (of dimensions ~ 0.1 mm \times 6 mm) on the films coated on the sample
33 slides, which were aligned perpendicular to the excitation stripe. The emission from the film
34 edge was collected in a lateral configuration by a pair of lenses focused onto an optical fiber
35 coupled to a spectrometer (Acton, Spectra Pro 2500i) and detected by a charge coupled device
36 (Princeton Instruments, PIXIS 400B CCD).
37
38
39
40
41
42
43
44

45 The two-photon pumped time resolved PL was detected by an Optronis OptoscopeTM streak
46 camera system which has an ultimate temporal resolution of ~ 6 ps when operated at the shortest
47 time window of 330 ps. Lastly, lasing from a single microsphere was observed using a home-
48 built confocal microscope with both the excitation pulses and emission light being coupled and
49 collected through the same long working distance 50 \times microscope objective (NA = 0.55); and
50 spectrally resolved by the abovementioned spectrometer and CCD detector.
51
52
53
54
55
56
57
58
59
60

1
2
3 For nanosecond TA experiments, a laser flash photolysis spectrometer (LKS.60, Applied
4 Photophysics), equipped with a Q-Switched Nd:YAG laser (Brilliant B, Quantel), a 150 W
5 pulsed Xe lamp and a R928 photomultiplier, was used to record ns-difference absorption spectra.
6
7
8 Samples were excited at 440 nm and each time-resolved trace was acquired by averaging 10 laser
9
10
11
12
13 shots at a repetition rate of 1 Hz.
14

15 16 17 AUTHOR INFORMATION

18 19 **Corresponding Authors**

20 *E-mail: tzechien@ntu.edu.sg; * E-mail: chmchany@nus.edu.sg
21
22
23
24

25 26 **Author Contributions**

27
28 §These authors contributed equally to this work.
29
30
31

32 33 34 ACKNOWLEDGMENT.

35 Financial support from NTU start-up grant M58110068, SPMS collaborative Research Award
36 M58110090, NUS start-up grant WBS-R143-000-367-133, A*STAR TSRP grant R143-000-
37 435-305, DSTA grant R143-000-423-422 is gratefully acknowledged. G. X., X. L., Y. C. and T.
38
39 C. S. acknowledge the financial support by the Singapore National Research Foundation (NRF)
40 through the Singapore-Berkeley Research Initiative for Sustainable Energy (SINBERISE)
41
42
43
44
45
46
47
48
49
50
51
52
53
54
55
56
57
58
59
60
61
62
63
64
65
66
67
68
69
70
71
72
73
74
75
76
77
78
79
80
81
82
83
84
85
86
87
88
89
90
91
92
93
94
95
96
97
98
99
100
101
102
103
104
105
106
107
108
109
110
111
112
113
114
115
116
117
118
119
120
121
122
123
124
125
126
127
128
129
130
131
132
133
134
135
136
137
138
139
140
141
142
143
144
145
146
147
148
149
150
151
152
153
154
155
156
157
158
159
160
161
162
163
164
165
166
167
168
169
170
171
172
173
174
175
176
177
178
179
180
181
182
183
184
185
186
187
188
189
190
191
192
193
194
195
196
197
198
199
200
201
202
203
204
205
206
207
208
209
210
211
212
213
214
215
216
217
218
219
220
221
222
223
224
225
226
227
228
229
230
231
232
233
234
235
236
237
238
239
240
241
242
243
244
245
246
247
248
249
250
251
252
253
254
255
256
257
258
259
260
261
262
263
264
265
266
267
268
269
270
271
272
273
274
275
276
277
278
279
280
281
282
283
284
285
286
287
288
289
290
291
292
293
294
295
296
297
298
299
300
301
302
303
304
305
306
307
308
309
310
311
312
313
314
315
316
317
318
319
320
321
322
323
324
325
326
327
328
329
330
331
332
333
334
335
336
337
338
339
340
341
342
343
344
345
346
347
348
349
350
351
352
353
354
355
356
357
358
359
360
361
362
363
364
365
366
367
368
369
370
371
372
373
374
375
376
377
378
379
380
381
382
383
384
385
386
387
388
389
390
391
392
393
394
395
396
397
398
399
400
401
402
403
404
405
406
407
408
409
410
411
412
413
414
415
416
417
418
419
420
421
422
423
424
425
426
427
428
429
430
431
432
433
434
435
436
437
438
439
440
441
442
443
444
445
446
447
448
449
450
451
452
453
454
455
456
457
458
459
460
461
462
463
464
465
466
467
468
469
470
471
472
473
474
475
476
477
478
479
480
481
482
483
484
485
486
487
488
489
490
491
492
493
494
495
496
497
498
499
500
501
502
503
504
505
506
507
508
509
510
511
512
513
514
515
516
517
518
519
520
521
522
523
524
525
526
527
528
529
530
531
532
533
534
535
536
537
538
539
540
541
542
543
544
545
546
547
548
549
550
551
552
553
554
555
556
557
558
559
560
561
562
563
564
565
566
567
568
569
570
571
572
573
574
575
576
577
578
579
580
581
582
583
584
585
586
587
588
589
590
591
592
593
594
595
596
597
598
599
600
601
602
603
604
605
606
607
608
609
610
611
612
613
614
615
616
617
618
619
620
621
622
623
624
625
626
627
628
629
630
631
632
633
634
635
636
637
638
639
640
641
642
643
644
645
646
647
648
649
650
651
652
653
654
655
656
657
658
659
660
661
662
663
664
665
666
667
668
669
670
671
672
673
674
675
676
677
678
679
680
681
682
683
684
685
686
687
688
689
690
691
692
693
694
695
696
697
698
699
700
701
702
703
704
705
706
707
708
709
710
711
712
713
714
715
716
717
718
719
720
721
722
723
724
725
726
727
728
729
730
731
732
733
734
735
736
737
738
739
740
741
742
743
744
745
746
747
748
749
750
751
752
753
754
755
756
757
758
759
760
761
762
763
764
765
766
767
768
769
770
771
772
773
774
775
776
777
778
779
780
781
782
783
784
785
786
787
788
789
790
791
792
793
794
795
796
797
798
799
800
801
802
803
804
805
806
807
808
809
810
811
812
813
814
815
816
817
818
819
820
821
822
823
824
825
826
827
828
829
830
831
832
833
834
835
836
837
838
839
840
841
842
843
844
845
846
847
848
849
850
851
852
853
854
855
856
857
858
859
860
861
862
863
864
865
866
867
868
869
870
871
872
873
874
875
876
877
878
879
880
881
882
883
884
885
886
887
888
889
890
891
892
893
894
895
896
897
898
899
900
901
902
903
904
905
906
907
908
909
910
911
912
913
914
915
916
917
918
919
920
921
922
923
924
925
926
927
928
929
930
931
932
933
934
935
936
937
938
939
940
941
942
943
944
945
946
947
948
949
950
951
952
953
954
955
956
957
958
959
960
961
962
963
964
965
966
967
968
969
970
971
972
973
974
975
976
977
978
979
980
981
982
983
984
985
986
987
988
989
990
991
992
993
994
995
996
997
998
999
1000

REFERENCES

1. Klimov, V. I.; Mikhailovsky, A. A.; Xu, S.; Malko, A.; Hollingsworth, J. A.; Leatherdate, C. A.; Eisler, H. -J.; Bawendi, M. G. Optical Gain and Stimulated Emission in Nanocrystal Quantum Dots. *Science* **2000**, *290*, 314-317.
2. Sundar, V. C.; Eisler, H. -J.; Bawendi, M. G. Room-Temperature, Tunable Gain Media from Novel II-VI Nanocrystal-Titania Composite Matrices. *Adv. Mater.* **2002**, *14*, 739-743.
3. Sundar, V. C.; Eisler, H. -J.; Deng, T.; Chan, Y.; Thomas, E. L.; Bawendi, M. G. Soft-Lithographically Embossed Multilayered Distributed-Feedback Nanocrystal Lasers. *Adv. Mater.* **2004**, *16*, 2137-2141.
4. Ivanov, S. A.; Nanda, J.; Piryatinski, A.; Achermann, M.; Balet, L. P.; Bezel, I. V.; Anikeeva, P. O.; Tretiak, S.; Klimov, V. I. Light Amplification Using Inverted Core/Shell Nanocrystals: Towards Lasing in the Single-Exciton Regime. *J. Phys. Chem. B* **2004**, *108*, 10625-10630.
5. Chan, Y.; Steckel, J. S.; Snee, P. T.; Caruge, J. -M.; Hodgkiss, J. M.; Nocera, D. G.; Bawendi, M. G. Blue Semiconductor Nanocrystal Laser. *Appl. Phys. Lett.* **2005**, *86*, 1/073102-3/073102.
6. Snee, P. T.; Chan, Y.; Nocera, D. G.; Bawendi, M. G. Whispering-Gallery-Mode Lasing from A Semiconductor Nanocrystal/Microsphere Resonator Composite. *Adv. Mater.* **2005**, *17*, 1131-1136.

1
2
3 7. Klimov, V. I.; Ivanov, S. A.; Nanda, J.; Achermann, M.; Bezel, I.; McGuire, J. A.;
4
5 Piryatinski, A. Single-Exciton Optical Gain in Semiconductor Nanocrystals. *Nature* **2007**, *447*,
6
7 441-446.
8
9

10
11 8. Zavelani-Rossi, M.; Lupo, M. G.; Krahn, R.; Manna, L.; Lanzani, G. Lasing in Self-
12
13 Assembled Microcavities of CdSe/CdS Core/Shell Colloidal Quantum Rods. *Nanoscale* **2010**, *2*,
14
15 931-935.
16
17

18
19 9. Dang, C.; Lee, J.; Breen, C.; Steckel, J. S.; Coe-Sullivan, S.; Nurmikko, A. Red, Green and
20
21 Blue Lasing Enabled by Single-Exciton Gain in Colloidal Quantum Dot Films. *Nat.*
22
23 *Nanotechnol.* **2012**, *7*, 335-339.
24
25

26
27 10. Cooney, R. R.; Sewall, S. L.; Sagar, D. M.; Kambhampati, P. Gain Control in
28
29 Semiconductor Quantum Dots *via* State-Resolved Optical Pumping. *Phys. Rev. Lett.* **2009**, *102*,
30
31 1/127404-4/127404.
32
33

34
35 11. Moreels, I.; Rainò, G.; Gomes, R.; Hens, Z.; Stöferle, T.; Mahrt, R. F. Nearly Temperature-
36
37 Independent Threshold for Amplified Spontaneous Emission in Colloidal CdSe/CdS Quantum
38
39 Dot-in-Rods. *Adv. Mater.* **2012**, *24*, OP231-5.
40
41

42
43 12. Todescato, F.; Fortunati, I.; Gardin, S.; Garbin, E.; Collini, E.; Bozio, R.; Jasieniak, J. J.;
44
45 Guistina, G. D.; Brusatin, G.; Toffanin, S.; *et al.* Soft-Lithographed Up-Converted Distributed
46
47 Feedback Visible Lasers Based on CdSe-CdZnS-ZnS Quantum Dots. *Adv. Funct. Mater.* **2012**,
48
49 *22*, 337-344.
50
51
52
53
54
55
56
57
58
59
60

- 1
2
3 13. Oohata, G.; Kagotani, Y.; Miyajima, K.; Ashida, M.; Saito, S.; Edamatsu, K.; Itoh, T.
4
5 Stable Biexcitonic Lasing of CuCl Quantum Dots under Two-Photon Resonant Excitation. *Phys.*
6
7 *E* **2005**, *26*, 347-350.
8
9
10
11 14. Jasieniak, J. J.; Fortunati, I.; Gardin, S.; Signorini, R.; Bozio, R.; Martucci, A.; Mulvaney,
12
13 P. Highly Efficient Amplified Stimulated Emission from CdSe-CdS-ZnS Quantum Dot Doped
14
15 Waveguides with Two-Photon Infrared Optical Pumping. *Adv. Mater.* **2008**, *20*, 69-73.
16
17
18
19 15. Zhang, C.; Zhang, F.; Zhu, T.; Cheng, A.; Xu, J.; Zhang, Q.; Mohny, S. E.; Henderson, R.
20
21 H.; Wang, Y. A. Two-Photon-Pumped Lasing from Colloidal Nanocrystal Quantum Dots. *Opt.*
22
23 *Lett.* **2008**, *33*, 2437-2439.
24
25
26
27 16. Zhang, C.; Zhang, F.; Cheng, A.; Kimball, B.; Wang, A. Y.; Xu, J. Frequency Upconverted
28
29 Lasing of Nanocrystal Quantum Dots in Microbeads. *Appl. Phys. Lett.* **2009**, *95*, 1/183109-
30
31 3/183109.
32
33
34
35 17. Wiersma, D. S. The Physics and Applications of Random Lasers. *Nature Phys.* **2008**, *4*,
36
37 359-367.
38
39
40
41 18. Pu, S. C.; Yang, M. J.; Hsu, C. C.; Lai, C. W.; Hsieh, C. C.; Lin, S. H.; Cheng, Y. M.;
42
43 Chou, P. T. The Empirical Correlation between Size and Two-Photon Absorption Cross Section
44
45 of CdSe and CdTe Quantum Dots. *Small* **2006**, *2*, 1308-1313.
46
47
48
49 19. He, G. S.; Yong, K. T.; Zheng, Q. D.; Sahoo, Y.; Baev, A.; Rysanyanskiy, A. I.; Prasad, P.
50
51 N. Multi-Photon Excitation Properties of CdSe Quantum Dots Solutions and Optical Limiting
52
53 Behavior in Infrared Range. *Opt. Express* **2007**, *15*, 12818-12833.
54
55
56
57
58
59
60

1
2
3 20. Xing, G.; Chakraborty, S.; Chou, K. L.; Mishra, N.; Huan, C. H. A.; Chan, Y.; Sum, T. C.
4
5 Enhanced Tunability of The Multiphoton Absorption Cross-Section in Seeded CdSe/CdS
6
7 Nanorod Heterostructures. *Appl. Phys. Lett.* **2010**, *97*, 1/061112-3/061112.
8
9

10
11 21. He, G. S.; Markowicz, P. P.; Lin, T. C.; Prasad, P. N. Observation of Stimulated Emission
12
13 by Direct Three-Photon Excitation. *Nature* **2002**, *415*, 767-770.
14
15

16
17 22. Carbone, L.; Nobile, C.; Giorgi, M. D.; Sala, F. D.; Morello, G.; Pompa, P.; Hytch, M.;
18
19 Snoeck, E.; Fiore, A.; Franchini, I. R.; *et al.* Synthesis and Micrometer-Scale Assembly of
20
21 Colloidal CdSe/CdS Nanorods Prepared by A Seeded Growth Approach. *Nano Lett.* **2007**, *7*,
22
23 2942-2950.
24
25

26
27 23. Deka, S.; Quarta, A.; Lupo, M. G.; Falqui, A.; Boninelli, S.; Giannini, C.; Morello, G.;
28
29 Giorgi, M. D.; Lanzani, G.; Spinella, C.; *et al.* CdSe/CdS/ZnS Double Shell Nanorods with High
30
31 Photoluminescence Efficiency and Their Exploitation As Biolabeling Probes. *J. Am. Chem. Soc.*
32
33 **2009**, *131*, 2948-2958.
34
35

36
37 24. Sitt, A.; Sala, F. D.; Menagen, G.; Banin, U. Multiexciton Engineering in Seeded
38
39 Core/Shell Nanorods: Transfer from Type-I to Quasi-Type-II Regimes. *Nano Lett.* **2009**, *9*, 3470-
40
41 3476.
42
43

44
45 25. Lupo, M. G.; Sala, F. D.; Carbone, L.; Zavelani-Rossi, M.; Fiore, A.; Lüer, L.; Polli, D.;
46
47 Cingolani, R.; Manna, L.; Lanzani, G. Ultrafast Electron-Hole Dynamics in Core/Shell
48
49 CdSe/CdS Dot/Rod Nanocrystals. *Nano Lett.* **2008**, *8*, 4582-4587.
50
51

52
53 26. Klimov, V. I. Spectral and Dynamical Properties of Multiexcitons in Semiconductor
54
55 Nanocrystals. *Annu. Rev. Phys. Chem.* **2007**, *58*, 635-673.
56
57
58
59
60

- 1
2
3 27. Beard, M. C.; Midgett, A. G.; Law, M.; Semonin, O. E.; Ellingson, R. J.; Nozik, A. J.
4 Variations in the Quantum Efficiency of Multiple Exciton Generation For A Series of
5 Chemically Treated PbSe Nanocrystal Films. *Nano Lett.* **2009**, *9*, 836-845.
6
7
8
9
10
11 28. Talapin, D. V.; Lee, J. S.; Kovalenko, M. V.; Shevchenko, E. V. Prospects of Colloidal
12 Nanocrystals for Electronic and Optoelectronic Applications. *Chem. Rev.* **2010**, *110*, 389-458.
13
14
15
16
17 29. Xing, G.; Ji, W.; Zheng, Y.; Ying, J. Y. Two- and Three-Photon Absorption of
18 Semiconductor Quantum Dots in the Vicinity of Half of Lowest Exciton Energy. *Appl. Phys.*
19 *Lett.* **2008**, *93*, 1/241114-3/241114.
20
21
22
23
24
25 30. Crooker, S. A.; Hollingsworth, J. A.; Tretiak, S.; Klimov, V. I. Spectrally Resolved
26 Dynamics of Energy Transfer in Quantum-Dot Assemblies: Towards Engineered Energy Flows
27 in Artificial Materials. *Phys. Rev. Lett.* **2002**, *89*, 1/186802-4/186802.
28
29
30
31
32
33 31. Lo, S. S.; Major, T. A.; Petchsang, N.; Huang, L. B.; Kuno, M. K.; Hartland, G. V. Charge
34 Carrier Trapping and Acoustic Phonon Modes in Single CdTe Nanowires. *ACS Nano* **2012**, *6*,
35 5274-5282.
36
37
38
39
40
41 32. Yan, Y.; Chen, G.; Van Patten, P. G.; Ultrafast Exciton Dynamics in CdTe Nanocrystals
42 and Core/Shell CdTe/CdS Nanocrystals. *J. Phys. Chem. C* **2011**, *115*, 22717-22728.
43
44
45
46 33. Sewall, S. L.; Cooney, R. R.; Anderson, K. E. H.; Dias, E. A.; Sagar, D. M.; Kambhampati,
47 P. State-Resolved Studies of Biexcitons and Surface Trapping Dynamics in Semiconductor
48 Quantum Dots. *J. Chem. Phys.* **2008**, *129*, 1/084701-8/084701.
49
50
51
52
53
54 34. Spillane, S. M.; Kippenberg, T. J.; Vahala, K. J. Ultralow-Threshold Raman Laser Using A
55 Spherical Dielectric Microcavity. *Nature* **2002**, *415*, 621-623.
56
57
58
59
60

1
2
3 35. Armani, D. K.; Kippenberg, T. J.; Spillane, S. M.; Vahala, K. J. Ultra-High-Q Toroid
4 Microcavity on A Chip. *Nature* **2003**, *421*, 925-928.
5
6
7
8
9
10

11
12 **Table I.** Average length, quantum yield (η), 2PA cross-section (σ_2), two-electron-hole pair decay
13 time (τ_2) and 2ASE threshold of CdSe/CdS nanodot/nanorod heterostructures.
14
15
16

length (nm)	η [%]	$\sigma_2^{\#}$ [GM]	τ_2 [ps]	Threshold [mJ/cm ²]
15	75	70000	190	3.4
34	61	190000	260	1.8
39	56	230000	300	1.5

17
18
19
20
21
22
23
24
25
26
27
28 [#]Experimental uncertainty: $\pm 20\%$.
29
30
31
32
33
34
35
36
37
38
39
40
41
42
43
44
45
46
47
48
49
50
51
52
53
54
55
56
57
58
59
60

Figures & Figure Captions:

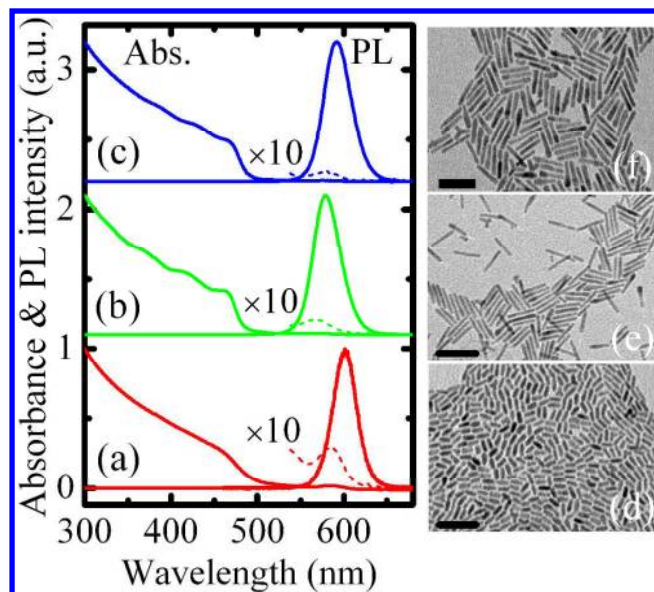


Figure 1. (a), (b) and (c) show the normalized UV-visible absorption spectra (solid line) and its magnified ($\times 10$) region (dashed line), 400 nm excited PL spectra for 15 nm, 34 nm and 39 nm CdSe/CdS nanodot/nanorod heterostructure respectively. (d), (e) and (f) show the corresponding TEM images, scale bars are 50 nm.

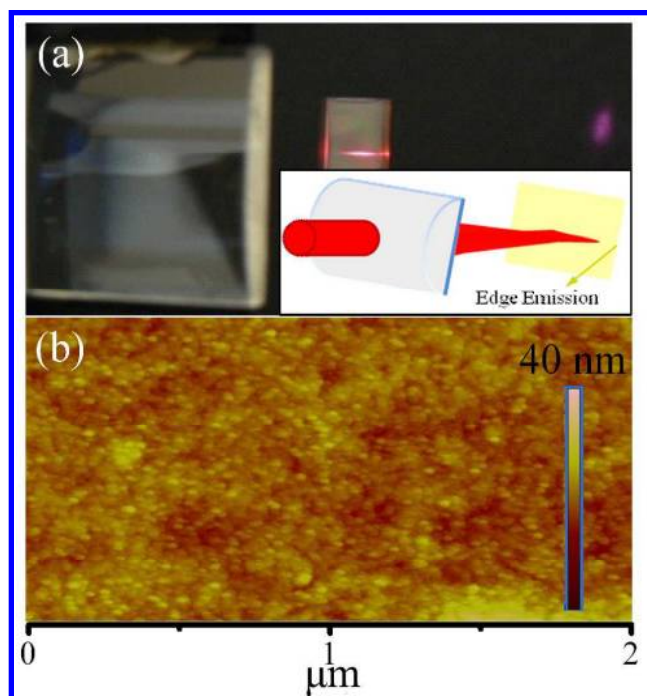


Figure 2. (a) A digital photograph of frequency-upconverted stimulated emission from CdSe/CdS heterostructures film, pumped by 2PA at 800 nm. Inset shows the pumping configuration. (b) Tapping-mode AFM image of the typical surface profile of the close packed CdSe/CdS heterostructure films.

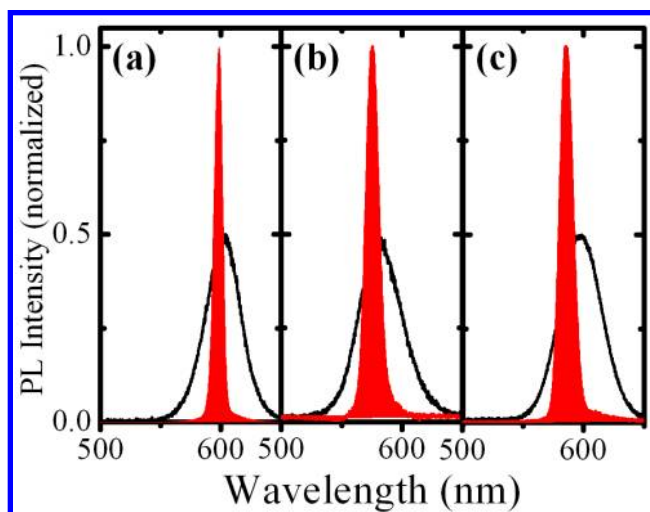


Figure 3. 2ASE spectra (**Red**) obtained from the films with 15 nm (**a**), 34 nm (**b**) and 39 nm (**c**) CdSe/CdS heterostructures at an 800 nm pump wavelength. The 2PA induced SE spectra (**Black**) are also shown for each corresponding sample.

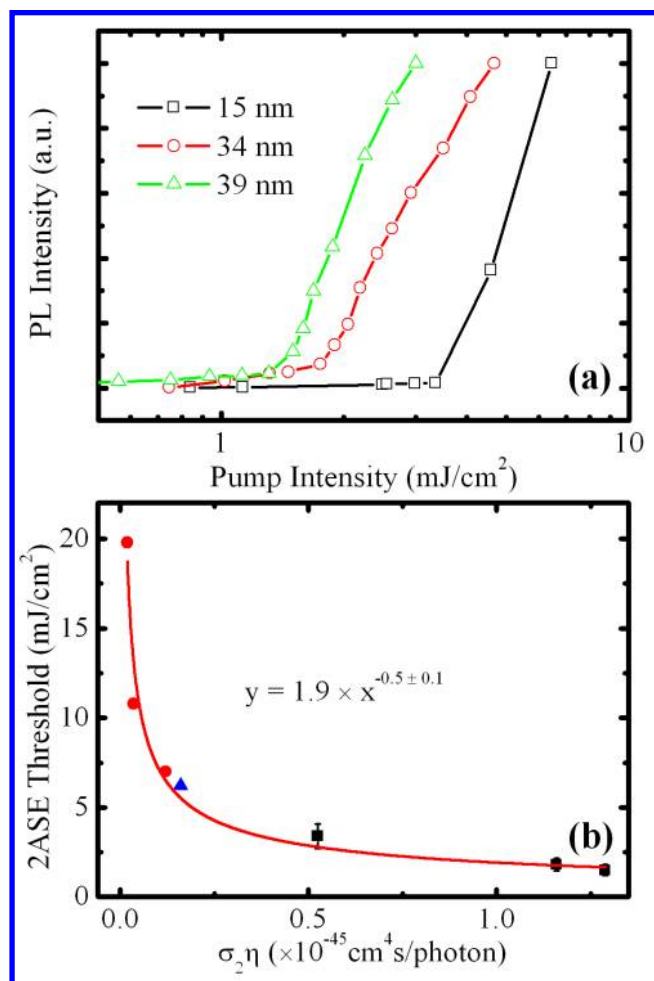


Figure 4. (a) Variable fluence measurements show the 2ASE thresholds of the CdSe/CdS heterostructures. (b) The plot of 2ASE vs. 2PA action cross-section ($\sigma_2\eta$). The experimental results were taken from present work (■), Ref. 14 (●) and Ref. 15 (▲). The red line is a power-law fitting.

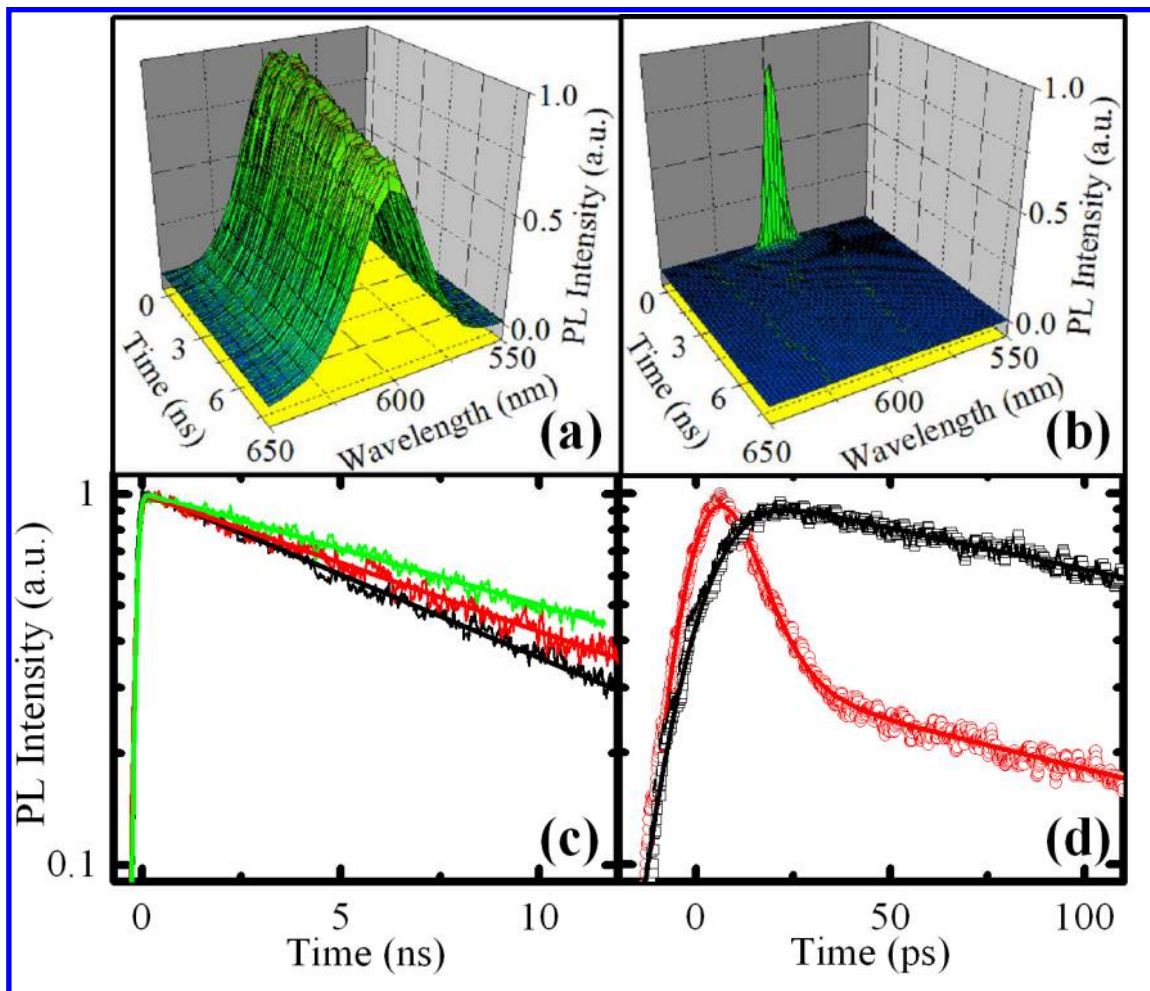


Figure 5. Typical 3D time-resolved 2PA induced SE (a) and ASE (b) spectra for 15 nm CdSe/CdS heterostructures film. (c) 2PA induced SE (integrated ± 5 nm around the emission peak) decay curves and the single-exponential fittings for 15 nm (black), 34 nm (red) and 39 nm (green) heterostructure films. (d) Typical time-resolved PL traces with 2PA excitation fluence just below (black) and above (red) the ASE threshold for the 15 nm heterostructure film.

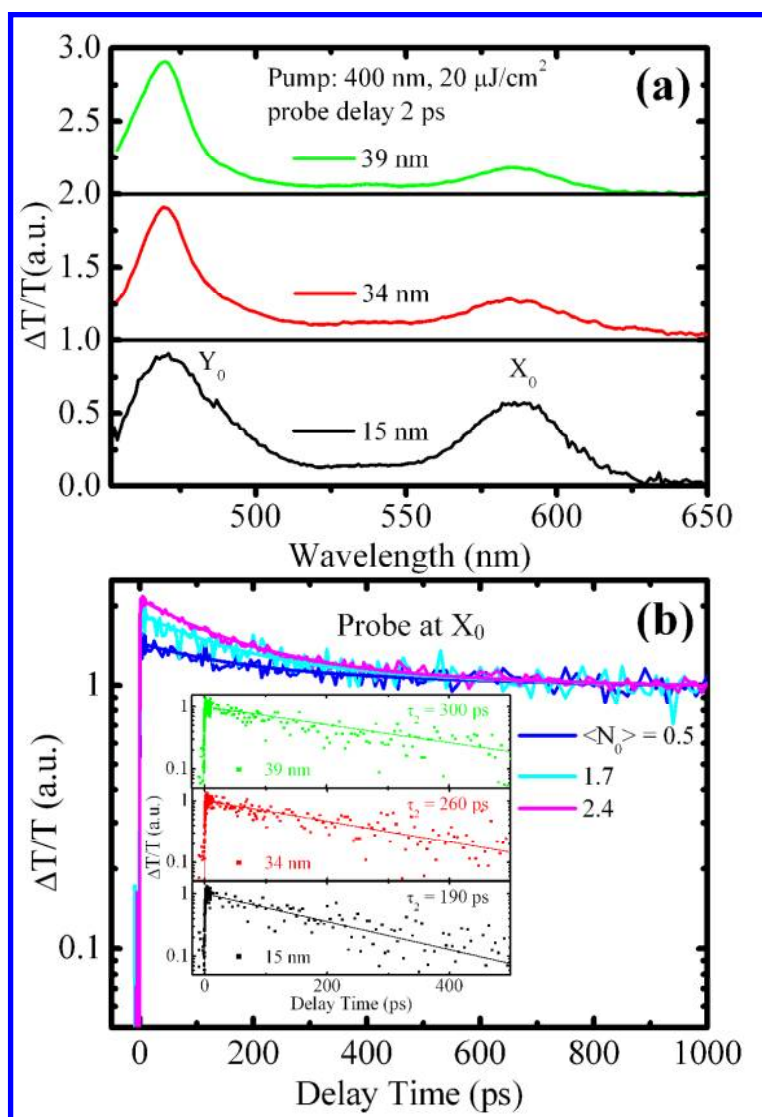


Figure 6. (a) Differential transmission spectra for the nano heterostructures in toluene solution at a probe delay of 2 ps. The bleaching peaks corresponding to the lowest lying energy levels in CdS and CdSe are labeled as Y_0 and X_0 , respectively. (b) Pump fluence-dependent decay transients of X_0 normalized to their long-lived decay component for the 15 nm CdSe/CdS nanorods. The inset show the decay transients of the two electron-hole pair states for the NRs with different lengths, fitted with a single exponential decay function (line).

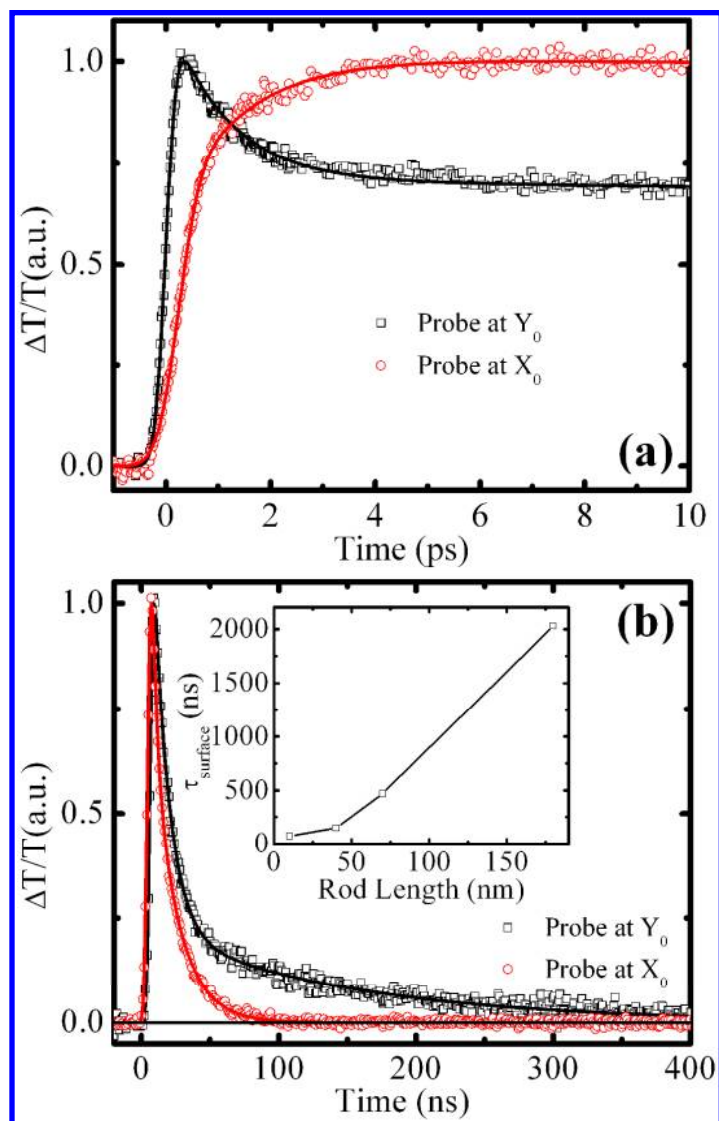


Figure 7. Normalized PB transients at X_0 and Y_0 shown with fs time resolution (a) and ns time resolution (b) for the 39 nm nano rod with an excitation fluence that produces ~ 1 e-h pair per rod. The inset shows the rod length dependent surface trapped hole decay lifetime for the heterostructures.

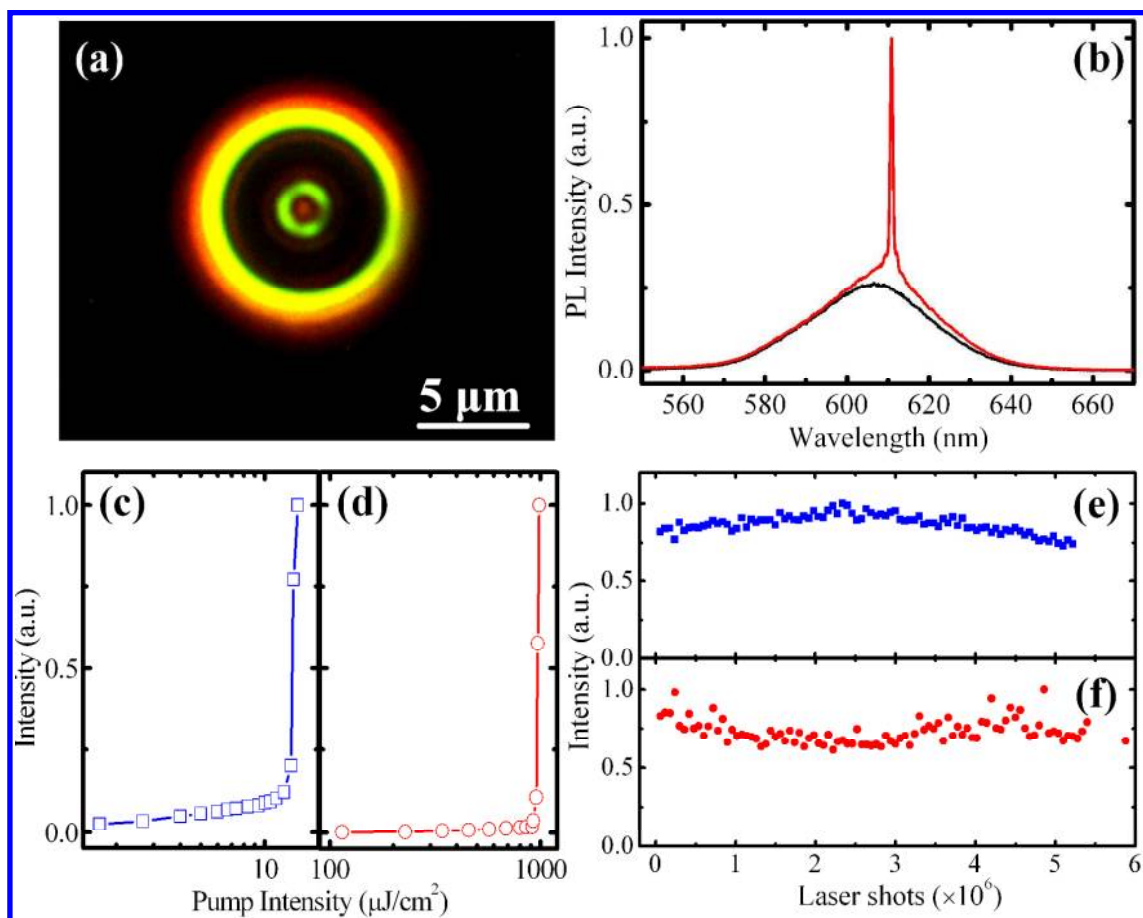


Figure 8. (a) An optical image of a 5 μm silica micro-sphere coated with a CdSe/CdS NRs silica film. (b) The spectra of a single 5 μm microsphere below ($800 \mu\text{J}/\text{cm}^2$) and above ($990 \mu\text{J}/\text{cm}^2$) laser threshold with two-photon pumping. The photoluminescence intensity as a function of pump intensity for one- (blue) (c) and two-photon (red) (d) pumping, respectively. Shot dependent lasing intensity of a microsphere under one- (e) and two-photon (f) pumping.

